Thermal evolution of internal strain in doped PbTe

James P. Male[1+], Riley Hanus[2*+], G. Jeffrey Snyder[1*], and Raphaël P. Hermann[2]

[1]Materials Science and Engineering, Northwestern University, Evanston, IL 60208, USA.
[2]Materials Science and Technology Division, Oak Ridge National Laboratory, Oak Ridge, TN 37831, USA.
[*]Corresponding author: hanusriley@gmail.com, jeff.snyder@northwestern.edu
[+]J.P.M. and R.H. contributed equally to this work

ABSTRACT

Recent improvements in the efficiency of heat-to-electricity energy conversion in lead chalcogenide thermoelectrics involve reducing the thermal conductivity by incorporating large amounts of internal strain. The extent to which typical lead chalcogenide processing techniques (such as doping, ball milling, and densification) increase internal strain and dislocation density must be quantified to improve materials design. In this study, neutron powder diffraction is leveraged to evaluate the internal strain introduced by ball milling in doped and undoped powders. Doping with Na and/or Eu increases internal strain beyond ball milling alone with the greatest increase from combining the two dopants. Strain recovery occurs in each powder above 400 K but can be suppressed by co-doping – indicating a strong dopant-dislocation interaction in this system. Therefore, high temperature processing of PbTe powders should be avoided if high internal strain is desired. Low temperature densification and/or rapid pressing techniques may be key to maintaining internal strain in the final pressed pellet. The diffraction peak asymmetry and correlated elastic softening measured in pressed PbTe pellets in past studies was not observed in the precursor powders measured here, suggesting that measurements of Debye temperature on final pressed pellets are required to examine the influence of defect induced elastic softening on thermal conductivity. This work provides key guidance for defect engineering to maximize internal strain and thermoelectric performance in PbTe thermoelectrics.

1 Introduction

Reducing the vibrational (lattice) thermal conductivity (κ_{vib}) has enabled record-breaking thermoelectric efficiencies in the past decade. Historic breakthroughs in raising the thermoelectric figure of merit (zT) in lead chalcogenides can be traced back to increased defect phonon scattering[1–5] and lattice softening[6–13] — or a reduction in phonon energy and group velocity with increased defect density and/or temperature. Internal strain has emerged as an important material property governing vibrational thermal conductivity and zT[10]. Defects of various dimension, like point defects, dislocations, and boundaries, can increase internal strain. In PbTe, dislocations appear to be most effective at increasing strain and reducing κ_{vib} without harming electronic transport[14,15], whereas point defects are limited by solubility and interfaces tend to reduce mobility[16,17].

Defect engineering is a promising materials design strategy for introducing phonon scattering centers and internal strain to improve zT[18,19]. When considering all possible chemical substitutions, defect reactions, experimental procedures, and resulting microstructures, the design space for defect engineering is vast. Therefore, detailed materials characterization throughout the synthesis process is important for designing better thermoelectrics. The routine synthesis for lead chalcogenide thermoelectrics typically includes three major steps: melt synthesis, powdering, and densification — each of which presents a new opportunity to engineer highly strained defects.

Synthesis of lead chalcogenides and other thermoelectric materials often begins with reacting elements under vacuum in a quartz ampule to achieve the desired phase. Point defects in the form of intrinsic lattice defects and extrinsic dopants are considered here to engineer κ_{vib}[19,20] and to control electronic carriers – a necessity for high zT in lead chalcogenides[21]. Processing methods like high energy ball-milling[6,22] are then used to powder the ingots while controlling particle size and increasing internal strain by introducing microstructural defects such as dislocations. The point defects introduced at the start will influence the defects that form during powdering. For example, point defects are known to pin dislocations, which inhibits their annihilation and recrystallization[23,24]. Powders are typically densified into pellets for characterization or use in modules by rapid hot pressing[25] or "spark plasma sintering"[26]. Pressing temperature, time, and pressure are tuned to both maximize electronic mobility and minimize κ_{vib} by, for example, maintaining (or possibly introducing) internal strain from dislocations and interfaces. Densification can also improve the thermal stability of dislocations, which is essential for maintaining high strain in thermoelectrics operating at high temperatures. Therefore, a careful study of the influence of chemical substitutions on the magnitude and thermal stability of internal strain at each processing step is necessary. This information can guide decisions surrounding materials chemistry and thermoelectric design.

In this study, PbTe-based powders based on high zT compositions[6,10,27,28] are probed by neutron diffraction during in

situ heating to directly quantify the effects of materials chemistry, processing, and temperature on internal strain. Powders include both undoped and Na/Eu doped PbTe ball-milled for 0, 2.5, 5, or 15 minutes. We find that high internal strain in ball milled powders anneals out at moderate temperatures. Adding Na and/or Eu dopants incrementally increases the room temperature strain beyond that reached by ball milling alone, and the two dopants combined aid in "freezing in" strain at high temperatures. We also analyze the Debye temperature θ_D from the temperature dependent Debye Waller factor and comment on the fundamental differences between θ_D measured *via* ultrasound, heat capacity and atomic displacement parameters, as well as notable differences in the character of strain observed in strained PbTe powders vs pellets. The resulting analysis shows that Na and Eu, when introduced together, are effective at increasing and stabilizing the internal strain in PbTe. This study serves as a guide outlining best practices for synthesizing highly strained PbTe with the goal of minimizing κ_{vib} and maximizing zT.

2 Results & discussion

Figure 1 shows two characteristic neutron diffraction patterns and GSAS-II[29] Rietveld refinements. The Figure 1 patterns were collected at 50 K and 500 K on Na-doped PbTe ($Pb_{0.98}Na_{0.02}Te$) powder ball milled for 15 minutes. A reduced scattering vector, Q, range is shown for clarity, but all data was collected up to $Q = 40$ Å^{-1} (real space lattice spacing $d \sim 0.16$ Å) and discernible peaks were refined up to $Q \sim 20$ Å^{-1} in most cases (see Figure S1). Full refinement statistics showing good fits are provided in Table S2 and Table S3, along with additional refined crystallographic parameters. Each diffraction peak corresponds to rock salt ($Fm\bar{3}m$) PbTe and neither Figure 1 nor the other patterns collected in this experiment show secondary phase peaks, suggesting full dopant solubility. Strain can be compared between two samples without a full refinement by simply investigating peak widths (see Figure 1 inset). Strain broadens diffraction peaks by compression and dilation of lattice plane spacing at different locations in the sample, especially at high Q. The strain broadening in the Figure 1 inset is relatively symmetrical in contrast to an asymmetric broadening observed in X-ray diffraction studies of some strained PbTe pellets[30].

Doping and ball milling cause the expected changes in PbTe's lattice constant, a (Figure 2). In undoped PbTe, a decreases slightly with increasing ball milling time (Figure S2), which may be indicative of higher intrinsic vacancy concentrations from ball milling. Doping with Na decreases a in ball milled samples while Eu doping increases a, as expected from the dopant ionic sizes[31]. Simultaneously doping with both elements nullifies the changes and returns a to that of undoped PbTe with no ball milling. We find the temperature dependence of a to be well described by $a(T) = 6.43 + 1.17 \times 10^{-4}$ T for undoped, unmilled PbTe. The corresponding room temperature coefficient of thermal expansion (CTE), 1.81×10^{-5} K^{-1}, is in good agreement with previous reports (2.17×10^{-5} K^{-1} from X-ray diffraction[32]). In each of the other samples studied, the room temperature CTE is within 10 % of undoped, unmilled PbTe, indicating that our processing methods are inconsequential for PbTe's CTE. See Figure S3 and Table S2 in the SI for full thermal expansion data.

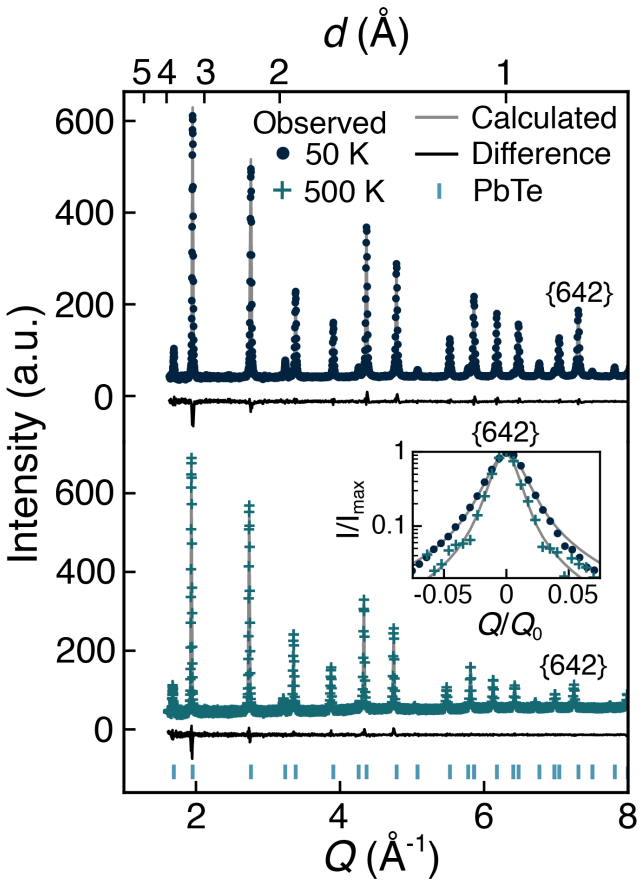

Figure 1. Characteristic neutron powder diffraction patterns at 50 K (top) and 500 K (bottom) taken on $Pb_{0.98}Na_{0.02}Te$ powder ball milled for 15 minutes. A calculated Rietveld refinement pattern is shown in gray, and the black lines below show the difference between observed and calculated data. All peaks correspond to PbTe crystallized in the rock salt ($Fm\bar{3}m$) structure with no secondary phase peaks. The inset highlights the high-Q {642} peak with background subtracted, which is qualitatively broader at 50 K, demonstrating much higher internal strain at low temperatures. Both scattering vector (Q) and lattice spacing (d) axes are provided.

Mean-square isotropic atomic thermal displacements, $\langle u^2 \rangle$, do not indicate major changes with strain at the accuracy of our measurement method. Figure 3 shows an example of nearly identical $\langle u^2 \rangle$ in undoped, unmilled PbTe and highly strained $Pb_{0.98}Na_{0.02}Te$ powders. Following a Debye-Waller type analysis[33], we calculate a Debye temperature for PbTe ($\theta_{D,PbTe}$) of 129(2) K for the undoped, unmilled powder and elemental Debye temperatures $\theta_{D,Pb}$ = 102(1) K and $\theta_{D,Te}$ = 163(2) K. In other samples, the same analysis reveals less

than 4% deviation from the Debye temperatures calculated for undoped, unmilled PbTe powder.

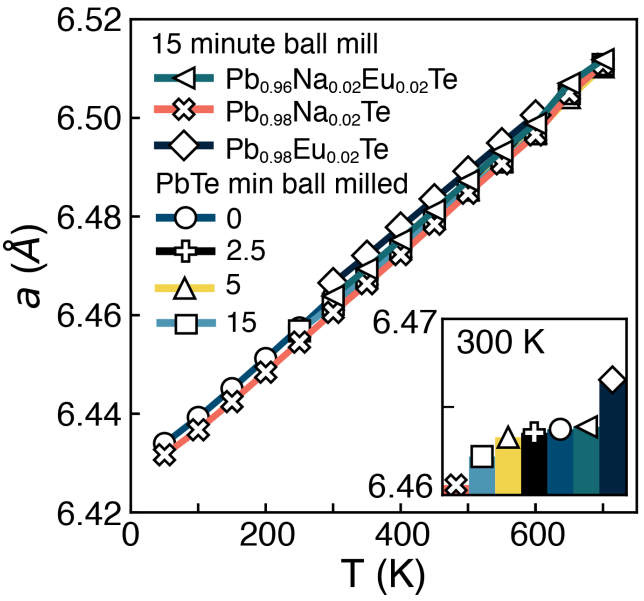

Figure 2. Temperature-dependent lattice constant (a) of undoped PbTe ball milled between 0-15 and PbTe doped with Eu and/or Na ball milled for 15 minutes. The inset highlights room temperature lattice constants. Measurement error listed in Table S2.

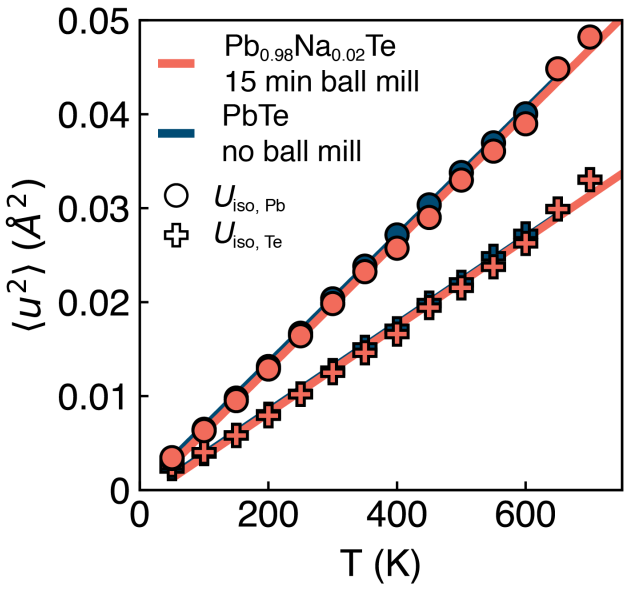

Figure 3. Temperature-dependent isotropic thermal displacement parameters ($\langle u^2 \rangle$) for Pb and Te in $Pb_{0.98}Na_{0.02}Te$ ball milled for 15 minutes (high internal strain) and undoped PbTe powder without ball milling (nominally unstrained). The linear fits used to calculate Debye temperatures for each sample are virtually equivalent.

Softening of PbTe's phonons is seemingly absent in strained powders based on our Debye-Waller analysis of thermal displacements (no appreciable softening of atomic displacements or θ_D with strain, see Figure S4). Elsewhere, speed of sound and low temperature heat capacity measurements find reduced θ_D (softening) in strained pellets[6–12]. X-ray diffraction showed that softening in strained PbTe pellets was accompanied by an asymmetric peak broadening with higher intensity on the large d-spacing side of the peak[6]. This asymmetric peak broadening is not observed in the powder samples (Figure 1 inset), indicating that the nature of internal strain in pressed pellets may differ from that in powder. Further, neutron (or X-ray) diffraction atomic displacement measurements are less sensitive to changes in low frequency phonons than speed of sound or low temperature heat capacity are[34–37]. Therefore, if internal strain is long range in PbTe, measuring atomic displacements with neutron diffraction may fail to capture softening of low frequency phonons. section S1 discusses in more detail which frequency ranges of the phonon density of states are probed by different experimental techniques (i.e. which *moment* each technique probes). Equivalence between different techniques to estimate θ_D should not always be expected. Indeed, when comparing θ_D values found for PbTe using varied methods (Table S1), our results agree well with measurements that probe a similar frequency range (i.e. Nuclear inelastic scattering atomic displacements), but not with others. From these observations, we conclude that elasticity, strain, and thermal conductivity measurements on the final pressed pellet are required to study defect induced lattice softening and atomic displacement measurements on strained pellets must be done to resolve whether the lack of softening in powders is due to choice of technique or a fundamental difference in the character of strain in powders versus pellets.

Internal strains calculated using Stephens' anisotropic strain model[38] show that ball milling and doping both introduce strain in PbTe (Figure S5). Unmilled, undoped PbTe powder contains $\sim$ 0.10 % strain between 50 - 600 K, and is used as a "nominally unstrained" reference point. Ball milling increases room temperature strain to $\sim$ 0.25 %, a more than 100 % increase. Strain saturates in as little as 2.5 minutes of ball milling and persists unchanged when continuing to 15 minutes (Figure S2). However, still longer times in the ball mill may begin to *reduce* strain, as observed in previous works[39]. Doping with 2 at. % of either Na or Eu causes $\sim$ 200 % higher strain relative to unstrained powder, with Eu being slightly more effective than Na. Combining the two elements brings strain to $\sim$ 300 % above the unstrained powder. Note that internal strain is uncorrelated with lattice parameter. After the strain is saturated, lattice constants continue to reduce with ball milling time. Additionally, no trend is apparent from decreased (Na), increased (Eu), or unchanged (Na and Eu) lattice constants in doped samples (Figure 2).

The large strain at or below room temperature rapidly disappears at moderate temperatures in all but the Eu/Na co-

doped PbTe powder, and Eu doping alone may reduce the rate of strain loss (Figure S5). Strain loss begins near 400 K during sample heating, which is remarkably similar to that observed in PbTe and other Pb chalcogenides in previous work[40]. The co-doped powder still contains 50 % more strain than unstrained PbTe after heating to 700 K, while the cooling data from the other strained powders shows a return to nominally unstrained levels. Data was not collected upon cooling for the Eu doped sample.

Internal strain from ball milling and doping in PbTe can be attributed to high dislocation concentrations and dopant-dislocation interactions. Stephens' model describes the anisotropic peak broadening in our cubic system with anisotropic strain parameters S_{220} and S_{400}[38] (tabulated in Table S3). We consistently find S_{220} to be approximately twice as high as S_{400}, leading to the anisotropic strain contour plots of Figure 5. Dimples along the principle axes and higher strain in the <110> directions are characteristic of strain from dislocations with Burgers vector $(a/2)$<110>, the dominant type in PbTe[24,30,41]. Consistent anisotropy between each sample suggests that doping does not change the type of dislocations present in the samples. Dislocations added by repetitive plastic deformation during ball milling saturate at a certain concentration in undoped PbTe, as evidenced by the upper strain limit in Figure S5b and Figure S2. Doping with Na and/or Eu raises strain beyond this limit, indicating that doped PbTe can sustain a higher dislocation concentration. This improvement is predictable – high dopant concentrations should lead to point defect-dislocation interactions. Additionally, some microscopy studies have found that certain dopants, like Na and Eu, tend to decorate dislocations in PbTe, creating Cottrell-like atmospheres in which impurity atoms segregate to dislocations and "freeze" them into the lattice[2,23,24]. Such mechanisms will hinder dislocation climb and annihilation, allowing larger strains to exist and restricting dislocations from annealing out at high temperature. Indeed, our co-doped powder has the highest strain and greatest strain-removal resilience at high temperatures, likely clarifying at least one reason for the conservation of low lattice thermal conductivity at high temperatures in Na/Eu co-doped PbTe pellets in other works[10]. It is therefore important to carefully choose dopants for maximizing and maintaining high temperature strain in PbTe. Dopants like Ag, Cu, and Ga were found to interact with dislocations in Pb chalcogenides and may therefore be particularly effective dopants for introducing strain and reducing thermal conductivity[24,27,42]. The advanced microstructure studies necessary to distinguish the distribution of dopants in PbTe are thus far limited. In most cases however, maximizing point defect concentrations without regard to specific doping mechanisms may be sufficient to reduce thermal conductivity through softening and scattering[43].

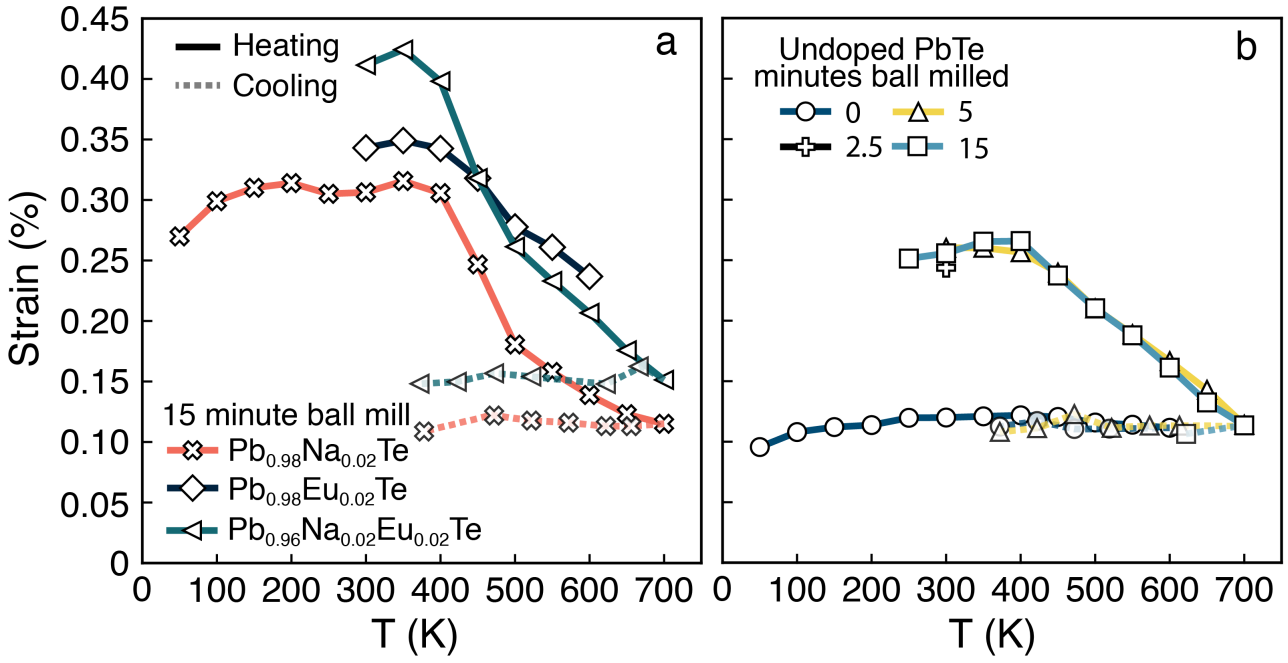

Figure 4. Temperature-dependent average strain of PbTe powders (a) doped with Na and/or Eu and ball milled for 15 minutes and (b) ball milled for varying times 0-15 minutes without doping. Data taken during both heating (solid lines) and cooling (dashed lines) are shown. Points on the cooling curve encompass 50 K binning around the plotted points.

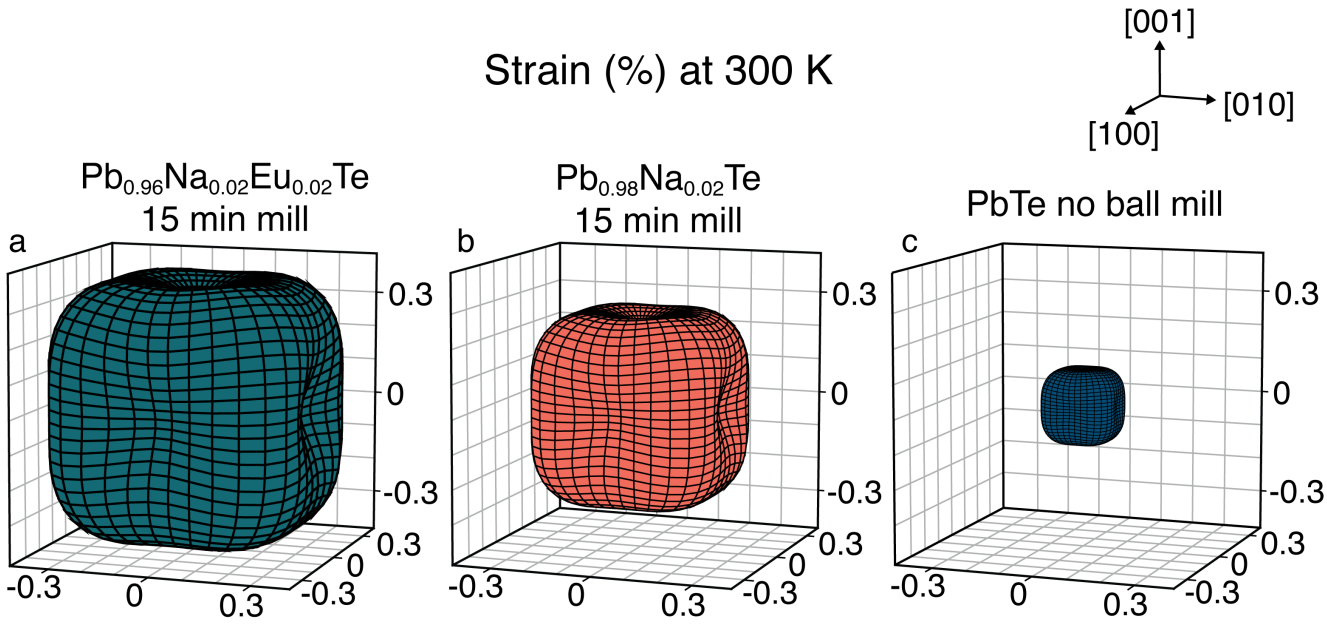

Figure 5. Selected strain contour plots obtained using the Stephen anisotropic strain model in GSAS-II refinements. The size of each volume represents overall strain, which is highest from (a) Na/Eu co-doping and ball milling ($Pb_{0.96}Na_{0.02}Eu_{0.02}Te$), slightly lower from (b) only Na doing in ball milled powders ($Pb_{0.98}Na_{0.02}Te$) and distinctly lower in (c) "nominally unstrained" PbTe powder prepared without ball milling. Strain is larger in the <110> directions than in the principal <h00> directions, as evidenced by strain surface dimples in the latter, indicating strain dominated by dislocations with Burgers vector (*a*/2)<110>.

The room temperature magnitude and temperature dependence of internal strain in powder samples is valuable for guiding materials processing, since it reveals the maximum temperature one should subject their powder to if internal strain in a pressed pellet is to be maximized. Powders prepared for this study were stored at room temperature for several months without losing strain, but significant strain annealed out during $\sim$ 30 minutes of measurement at $T \geq 400$ K. Therefore, strain loss occurs rapidly above room temperature and even short-term PbTe powder processing at moderate temperatures may nullify attempts to add strain during synthesis. Given that high strain in pressed PbTe pellets leads to softening and low κ_{vib}, removing strain from powder precursors may ultimately harm thermoelectric performance We note that the temperature dependence of internal strain in pellets is likely different than that observed in powders, and mechanisms such as dislocation pile-up at grain boundaries are expected to increase a pressed pellet's ability to maintain internal strain. Indeed, intentionally strained PbTe pellets measured by X-ray diffraction appear more resilient to strain loss after annealing[9,10] than the powders in this study and Abdellaoui *et al.* provided *in situ* transmission electron microscopy that shows that dislocations residing in Cottrell atmospheres in a pellet can be stable up to 523 K[23]. While the powders in this study were single phase, strain and thermal conductivity in Pb chalcogenide systems with secondary phases may also be strongly influenced by precipitation and nanostructuring – the character of which will be strongly dependent on the material's thermal processing history[44,45].

3 Conclusions

We explored the introduction and stability of internal strain during the standard melt-mill-sinter thermoelectric material synthesis procedure by in situ temperature-dependent neutron powder diffraction. We find that melting (doping) and milling (high-energy ball milling) each provide opportunities to add large degrees of internal strain to PbTe. However, most of the internal strain anneals out of the powders at moderate temperatures. A combination of Na and Eu dopants provides the greatest resistance to strain loss through strengthened defect-dislocation interactions, but fails to maintain initial levels of strain after brief times at elevated temperature. Internal strain seems better preserved at high temperatures after pressing (sintering) strained powders into pellets based on other works. This work reveals that further innovation in low temperature and rapid densification techniques may yield even larger reductions in thermal conductivity and improvements in thermoelectric conversion efficiency.

4 Experimental methods

4.1 PbTe synthesis

Undoped or Eu/Na doped PbTe ingots were synthesized by a melt-quench technique. Target stoichiometries of PbTe,

$Pb_{0.98}Na_{0.02}Te$, $Pb_{0.98}Eu_{0.02}Te$, or $Pb_{0.96}Na_{0.02}Eu_{0.02}Te$ were weighted in an Ar-filled glovebox (Pb shot, 99.999 % 5N+, USA; Te shot, 99.999 % 5N+, USA; shaved Na block 99.9 % Alfa Aesar, USA; Eu shot 99.9 % Alfa Aesar, USA) and enclosed in carbon-coated fused quartz ampoules, which were evacuated to $\sim 10^{-5}$ torr and flame sealed. The ampoules were heated in vertical tube furnaces from RT to 1273 K at 100 K/hr, where they were soaked for approximately 1 hour. The samples were then removed from the furnace and allowed to air quench.

One undoped PbTe ingot was lightly powdered by hand in a mortar and pestle to form a nominally "unstrained" powder. Other samples were strained by high energy ball milling in a Spex 8000D two-handed ball mill. Internal strain from ball milling can vary based on the mass and form factor of the starting material, the ball mill jar dimensions, and the number and size of balls added[6]. For consistency, ingot samples of identical mass (7.5 g) were each milled in the same stainless steel jar (36.7 mm diameter and 57 mm height, internal) with the same stainless steel balls (two 12.7 mm diameter and fifteen 6.3 mm diameter balls) and sealed in Ar before milling. Undoped ingots were ball milled for 2.5, 5, 7.5, or 15 minutes, and ingots with Na and/or Eu were ball milled for 15 minutes, with longer ball milling times expected to add more internal strain in each case.

4.1.1 Neutron diffraction

Temperature-dependent neutron powder diffraction measurements were performed at the POWGEN instrument at the Spallation Neutron Source (SNS) of Oak Ridge National Lab[46]. Frame 2 with 0.8 Å center wavelength was used. Vanadium cans containing about 2 cm^3 of PbTe powder were loaded into the cryofurnace sample environment using the high temperature JANIS stick. Empty vanadium cans were measured for background subtraction. Most samples were heated from room temperature to 700 K with pauses every 50 K for a $\sim$ 30 minute data collection. The Na doped and unmilled, undoped PbTe samples were cooled to 50 K before heating.

Data on most samples was collected continuously during cooling. Refinements at specific cooling temperature steps were performed by binning data on a 50 K grid during data reduction. This wide temperature range increases uncertainty in the cooling data. However, error in our cooling strain values likely overestimates the true value because slight changes to the lattice constant across the measurement temperature range will manifest as peak broadening. Our conclusion that strain is reduced upon cooling is therefore unaffected.

4.1.2 Crystallographic refinements and analysis

Neutron powder diffraction data was first reduced to a workable size and vanadium can backgrounds were subtracted using Mantid[47]. The reduced data was refined using GSAS-II[29] to extract crystallographic information. Instrument profile parameters based on a standard were provided by the POWGEN beamline scientists and used without change to ensure no cross-correlation between instrument broadening and strain broadening in the diffraction peaks. Much discussion surrounds the origins of low thermal conductivity in PbTe, with some authors focusing on correlated displacements, disorder, and/or anharmonicity[40,48–52]. Experimental evidence for such effects is often bolstered by advanced crystallographic studies including pair distribution function analysis of the diffuse signal. Identifying these effects is beyond the scope of this paper, which is concerned with extracting strain and isotropic thermal displacement information from Bragg peaks. As such, undulating patterns in the diffuse signal of each diffraction pattern were subtracted out by doing an ln-interpolate background fit with as many points as necessary for close fitting. After manual background fitting, the lattice constant and isotropic thermal displacement parameters were refined separately. The crystallite size was then set to its maximum of 10 μm, and strain parameters were refined along with both lattice constant and thermal displacements. Crystallite size remained near 10 μm after each refinement with uncertainties far exceeding 100% of the refined value, indicating that size broadening was insignificant in each fit. Stephens' generalized anisotropic strain method[38] was used in GSAS-II in accordance with past studies[6,40] to provide a better fit of PbTe's peak-dependent strain broadening than isotropic methods. The model also captures the character of the dominant $(a/2)$<110> burgers vector on PbTe dislocations (Figure 5). All the aforementioned properties were then refined together and the resulting microstrain value was noted. Microstrain was manually removed, and the process was repeated a second time, starting from the lattice constant refinement, to ensure no local minima were giving artificially high strain values. Repeating the process consistently reproduced near-identical results to the first refinement.

5 Supporting Information

Full Q range of example neutron diffraction pattern, strain and lattice constant as a function of ball milling time, thermal expansion analysis, thermal displacements as a function of strain, discussion on phonon dispersion moments and Debye temperatures, and tables containing full crystallographic information and refinement statistics.

6 Acknowledgements

We acknowledge the kind assistance of Dr. Qiang Zhang and Dr. Melanie Kirkham in carrying out measurements at the POWGEN instrument. This work was supported by the U.S. Department of Energy (DOE), Office of Science, Basic Energy Sciences, Materials Sciences and Engineering Division (neutron diffraction). RH acknowledges the DOE Science Graduate Research Award program (2018 Solicitation 2). Work by JM was supported by a NASA Space Technology Graduate Research Opportunity. GJS thanks award 70NANB19H005 from U.S. Department of Commerce, National Institute of Standards and Technology as part of the Center for Hierarchical Materials Design (CHiMaD). Research at ORNL's Spallation Neutron Source was sponsored by the Scientific User Facilities Division, Office of Basic Energy Sciences, U.S. Department of Energy.

References

1. Zhao, L. D., Dravid, V. P. & Kanatzidis, M. G. The panoscopic approach to high performance thermoelectrics, DOI: 10.1039/c3ee43099e (2014).
2. Biswas, K. *et al.* High-performance bulk thermoelectrics with all-scale hierarchical architectures. *Nature* **489**, 414–418, DOI: 10.1038/nature11439 (2012).
3. Tan, G. & Kanatzidis, M. G. All-Scale hierarchical PbTe: From nanostructuring to a panoscopic material. In Uher, C. (ed.) *Materials Aspect of Thermoelectricity*, chap. 4, 125–157, DOI: 10.1201/9781315197029 (CRC Press, Boca Raton, 2016).
4. Liu, Z., Mao, J., Liu, T. H., Chen, G. & Ren, Z. Nano-microstructural control of phonon engineering for thermoelectric energy harvesting. *MRS Bull.* **43**, 181–186, DOI: 10.1557/mrs.2018.7 (2018).
5. Kanatzidis, M. G. Nanostructured thermoelectrics: The new paradigm? *Chem. Mater.* **22**, 648–659, DOI: 10.1021/cm902195j (2010).
6. Hanus, R. *et al.* Lattice Softening Significantly Reduces Thermal Conductivity and Leads to High Thermoelectric Efficiency. *Adv. Mater.* **31**, 1900108, DOI: 10.1002/adma.201900108 (2019).
7. Tan, G. *et al.* High Thermoelectric Performance in SnTe- AgSbTe 2 Alloys from Lattice Softening, Giant Phonon-Vacancy Scattering, and Valence Band Convergence. *ACS Energy Lett.* **3**, 705–712, DOI: 10.1021/acsenergylett.8b00137 (2018).
8. Slade, T. J. *et al.* Contrasting SnTe-NaSbTe2and SnTe-NaBiTe2Thermoelectric Alloys: High Performance Facilitated by Increased Cation Vacancies and Lattice Softening. *J. Am. Chem. Soc.* **142**, 12524–12535, DOI: 10.1021/jacs.0c05650 (2020).
9. Wu, Y. *et al.* Manipulation of Band Degeneracy and Lattice Strain for Extraordinary PbTe Thermoelectrics. *Research* **2020**, 1–12, DOI: 10.34133/2020/8151059 (2020).
10. Wu, Y. *et al.* Lattice Strain Advances Thermoelectrics. *Joule* **3**, 1276–1288, DOI: 10.1016/j.joule.2019.02.008 (2019).
11. Chen, Z. *et al.* Lattice Dislocations Enhancing Thermoelectric PbTe in Addition to Band Convergence. *Adv. Mater.* **29**, 1–8, DOI: 10.1002/adma.201606768 (2017).
12. Lee, M. H., Park, J. H., Park, S. D., Rhyee, J. S. & Oh, M. W. Grain growth mechanism and thermoelectric properties of hot press and spark plasma sintered Na-doped PbTe. *J. Alloy. Compd.* **786**, 515–522, DOI: 10.1016/j.jallcom.2019.01.387 (2019).
13. Slade, T. J. *et al.* Charge-carrier-mediated Lattice Softening Contributes to High zT in Thermoelectric Semiconductors. *Joule* **5**, 1–15, DOI: 10.1016/j.joule.2021.03.009 (2021).
14. Chen, Z. *et al.* Vacancy-induced dislocations within grains for high-performance PbSe thermoelectrics. *Nat. Commun.* **8**, 1–8, DOI: 10.1038/ncomms13828 (2017).
15. Allgaier, R. S. & Scanlon, W. W. Mobility of Electrons and Holes in PbS, PbSe, and PbTe between Room Temperature and 4.2 K. *Phys. Rev.* **111**, 1029–1037, DOI: 10.1103/PhysRev.111.1029 (1958).
16. Zhu, T. *et al.* Compromise and Synergy in High-Efficiency Thermoelectric Materials. *Adv. Mater.* **29**, DOI: 10.1002/adma.201605884 (2017).
17. Kishimoto, K., Yamamoto, K. & Koyanagi, T. Influences of potential barrier scattering on the thermoelectric properties of sintered n-type PbTe with a small grain size. *Jpn. J. Appl. Physics, Part 1: Regul. Pap. Short Notes Rev. Pap.* **42**, 501–508, DOI: 10.1143/jjap.42.501 (2003).
18. Adamczyk, J. M. *et al.* Native Defect Engineering in CuInTe2. *Chem. Mater.* **33**, 359–369, DOI: 10.1021/acs.chemmater.0c04041 (2021).
19. Zhou, C. *et al.* Defect Engineering for High-Performance n-Type PbSe Thermoelectrics. *J. Am. Chem. Soc.* **140**, 9282–9290, DOI: 10.1021/jacs.8b05741 (2018).
20. He, J. *et al.* On the origin of increased phonon scattering in nanostructured pbte based thermoelectric materials. *J. Am. Chem. Soc.* **132**, 8669–8675, DOI: 10.1021/ja1010948 (2010).
21. Male, J. *et al.* The importance of phase equilibrium for doping efficiency: Iodine doped PbTe. *Mater. Horizons* **6**, 1444–1453, DOI: 10.1039/c9mh00294d (2019).
22. Rojas-Chávez, H. *et al.* The high-energy milling process as a synergistic approach to minimize the thermal conductivity of PbTe nanostructures. *J. Alloy. Compd.* **820**, 153167, DOI: 10.1016/j.jallcom.2019.153167 (2020).

23. Abdellaoui, L. *et al.* Parallel Dislocation Networks and Cottrell Atmospheres Reduce Thermal Conductivity of PbTe Thermoelectrics. *Adv. Funct. Mater.* 2101214, DOI: 10.1002/adfm.202101214 (2021).

24. Yu, Y. *et al.* Ag-Segregation to Dislocations in PbTe-Based Thermoelectric Materials. *ACS Appl. Mater. Interfaces* **10**, 3609–3615, DOI: 10.1021/acsami.7b17142 (2018).

25. LaLonde, A. D., Ikeda, T. & Snyder, G. J. Rapid consolidation of powdered materials by induction hot pressing. *Rev. Sci. Instruments* **82**, 025104, DOI: 10.1063/1.3534080 (2011).

26. Munir, Z. A., Anselmi-Tamburini, U. & Ohyanagi, M. The effect of electric field and pressure on the synthesis and consolidation of materials: A review of the spark plasma sintering method. *J. Mater. Sci.* **41**, 763–777, DOI: 10.1007/s10853-006-6555-2 (2006).

27. Deng, P. Y., Wang, K. K., Du, J. Y. & Wu, H. J. From Dislocation to Nano-Precipitation: Evolution to Low Thermal Conductivity and High Thermoelectric Performance in n-Type PbTe. *Adv. Funct. Mater.* **30**, 2005479, DOI: 10.1002/adfm.202005479 (2020).

28. Wang, X. *et al.* Sodium Substitution in Lead Telluride. *Chem. Mater.* **30**, 1362–1372, DOI: 10.1021/acs.chemmater.7b05091 (2018).

29. Toby, B. H. & Von Dreele, R. B. GSAS-II: The genesis of a modern open-source all purpose crystallography software package. *J. Appl. Crystallogr.* **46**, 544–549, DOI: 10.1107/S0021889813003531 (2013).

30. Hanus, R. *Heat Conduction in Defective and Complex Crystals : Phonon Scattering and Beyond*. Ph.D. thesis, Northwestern University (2019).

31. Shannon, R. D. Revised Effective Ionic Radii and Systematic Studies of Interatomic Distances in Halides and Chalcogenides. *Acta Cryst* **32**, 751–766 (1976).

32. Wang, X. K., Veremchuk, I., Bobnar, M., Zhao, J. T. & Grin, Y. Solid solution Pb1-XEuxTe: Constitution and thermoelectric behavior. *Inorg. Chem. Front.* **3**, 1152–1159, DOI: 10.1039/c6qi00161k (2016).

33. Möchel, A. *et al.* Lattice dynamics and anomalous softening in the YbFe4Sb 12 skutterudite. *Phys. Rev. B - Condens. Matter Mater. Phys.* **84**, 1–9, DOI: 10.1103/PhysRevB.84.184306 (2011).

34. Barron, T. H. K. & Morrison, J. A. On the specific heat of solids at low temperatures. *Can. J. Phys.* **35**, 799–810, DOI: 10.1139/p57-088 (1957).

35. Barron, T. H. K., Leadbetter, A. J., Morrison, J. A. & Salter, L. S. The calculation of Debye-Waller factors from thermodynamic data. In *Inelastic Scattering of Neutrons in Solids and Liquids*, 49–57 (1962).

36. Barron, T. H. K., Leadbetter, A. J., Morrison, J. A. & Salter, L. S. Temperature factors and thermodynamic properties of crystals. *Acta Crystallogr.* **20**, 125–131, DOI: 10.1107/s0365110x66000227 (1966).

37. Grimvall, G. Thermophysical Properties of Materials - Enlarged and revised edition. 89–97 (Elsevier Science B.V., 1999).

38. Stephens, P. W. Phenomenological model of anisotropic peak broadening in powder diffraction, DOI: 10.1107/S0021889898006001 (1999).

39. Bouad, N., Chapon, L., Marin-Ayral, R. M., Bouree-Vigneron, F. & Tedenac, J. C. Neutron powder diffraction study of strain and crystallite size in mechanically alloyed PbTe. *J. Solid State Chem.* **173**, 189–195, DOI: 10.1016/S0022-4596(03)00017-3 (2003).

40. Christensen, S., Bindzus, N., Sist, M., Takata, M. & Iversen, B. B. Structural disorder, anisotropic micro-strain and cation vacancies in thermo-electric lead chalcogenides. *Phys. Chem. Chem. Phys.* **18**, 15874–15883, DOI: 10.1039/c6cp01730d (2016).

41. Hirth, J. & Lothe, J. Theory of Dislocations. 285 (Wiley, New York, 1982), 2nd edn.

42. Zhou, C. *et al.* Exceptionally high average power factor and thermoelectric figure of merit in n-type PbSe by the dual incorporation of Cu and Te. *J. Am. Chem. Soc.* **142**, 15172–15186, DOI: 10.1021/jacs.0c07712 (2020).

43. Tang, J. *et al.* Atomic disordering advances thermoelectric group IV telluride alloys with a multiband transport. *Mater. Today Phys.* **15**, 1–7, DOI: 10.1016/j.mtphys.2020.100247 (2020).

44. Byrnes, J., Mitchell, D. R. & Aminorroaya Yamini, S. Thermoelectric performance of thermally aged nanostructured bulk materials—a case study of lead chalcogenides. *Mater. Today Phys.* **13**, 100190, DOI: 10.1016/j.mtphys.2020.100190 (2020).

45. Ren, F. *et al.* In situ neutron scattering study of nanoscale phase evolution in PbTe-PbS thermoelectric material. *Appl. Phys. Lett.* **109**, DOI: 10.1063/1.4961677 (2016).

46. Huq, A. *et al.* POWGEN: Rebuild of a third-generation powder diffractometer at the Spallation Neutron Source. *J. Appl. Crystallogr.* **52**, 1189–1201, DOI: 10.1107/S160057671901121X (2019).

47. Arnold, O. *et al.* Mantid - Data analysis and visualization package for neutron scattering and μ SR experiments. *Nucl. Instruments Methods Phys. Res. Sect. A: Accel. Spectrometers, Detect. Assoc. Equip.* **764**, 156–166, DOI: 10.1016/j.nima.2014.07.029 (2014).

48. Sangiorgio, B. *et al.* Correlated local dipoles in PbTe. *Phys. Rev. Mater.* **2**, 85402, DOI: 10.1103/PhysRevMaterials.2.085402 (2018).

49. Božin, E. S. *et al.* Entropically stabilized local dipole formation in lead chalcogenides. *Science* **330**, 1660–1663, DOI: 10.1126/science.1192759 (2010).

50. Shiga, T., Murakami, T., Hori, T., Delaire, O. & Shiomi, J. Origin of anomalous anharmonic lattice dynamics of lead telluride. *Appl. Phys. Express* **7**, 041801, DOI: 10.7567/APEX.7.041801 (2014).

51. Li, C. W. *et al.* Phonon self-energy and origin of anomalous neutron scattering spectra in SnTe and PbTe thermoelectrics. *Phys. Rev. Lett.* **112**, DOI: 10.1103/PhysRevLett.112.175501 (2014).

52. Li, C. W. *et al.* Anharmonicity and atomic distribution of SnTe and PbTe thermoelectrics. *Phys. Rev. B - Condens. Matter Mater. Phys.* **90**, 214303, DOI: 10.1103/PhysRevB.90.214303 (2014).

Supplementary Information: Thermal evolution of internal strain in doped PbTe

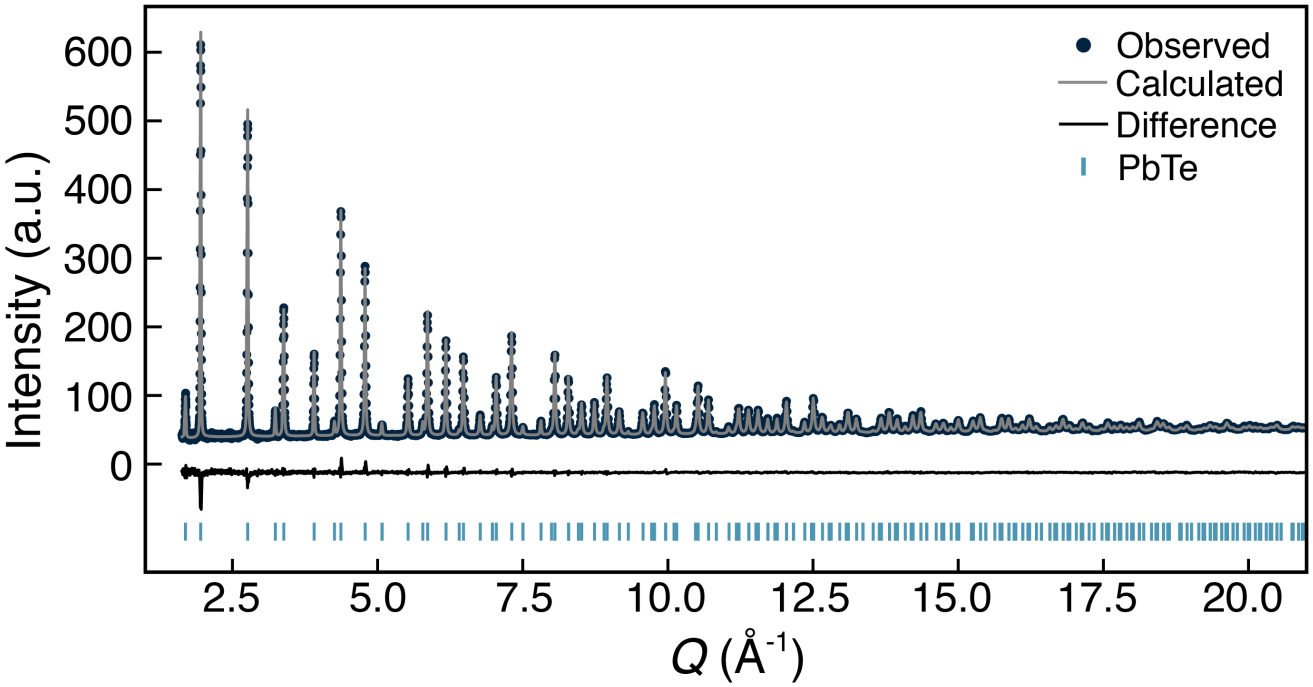

Figure S1. Neutron diffraction pattern taken on $Pb_{0.98}Na_{0.02}Te$ powder ball milled for 15 minutes showing full Q range used for Rietveld Refinement in GSAS-II. Discernible peaks from the rock salt PbTe structure ($Fm\bar{3}m$) are refined up to Q near 20 $Å^{-1}$. wR for this fit is 1.51, and refinements at higher temperature tend to have improved statistics.

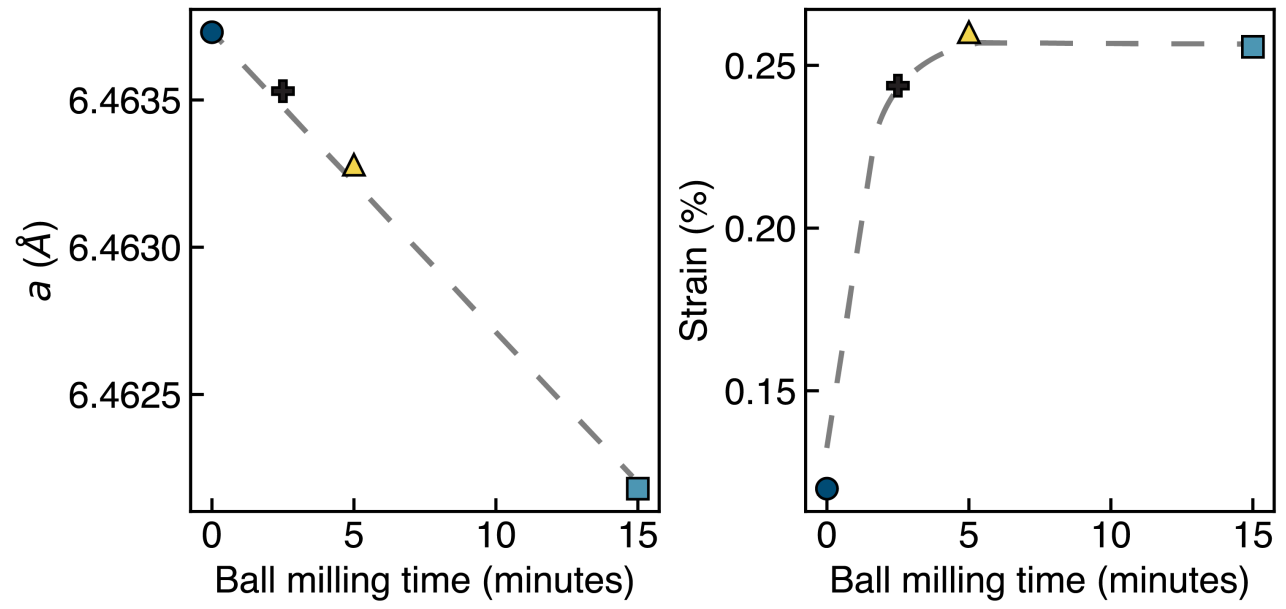

Figure S2. (a) Room temperature lattice parameter (a) and (b) strain in undoped PbTe powders high energy ball milled for 0, 2.5, 5, or 15 minutes. The a decreases linearly with ball milling time, while strain determined by Rietveld refinement saturates between 2.5 and 5 minutes of ball milling. Dotted lines are drawn as guides to the eye.

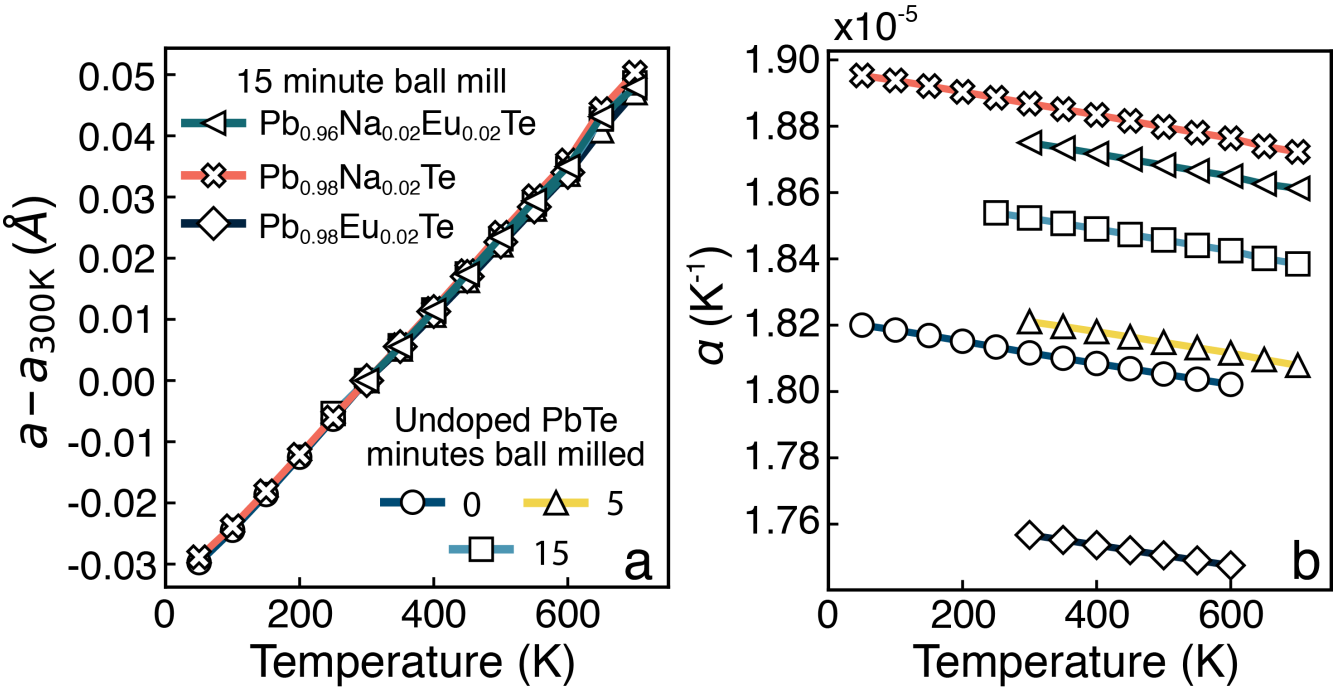

Figure S3. (a) Temperature dependent change in lattice parameter (a) relative to a at 300 K (a_{300K}). (b) First order coefficient of thermal expansion (α) and its temperature dependence. Each sample has α within 10 % of the undoped, unmilled sample.

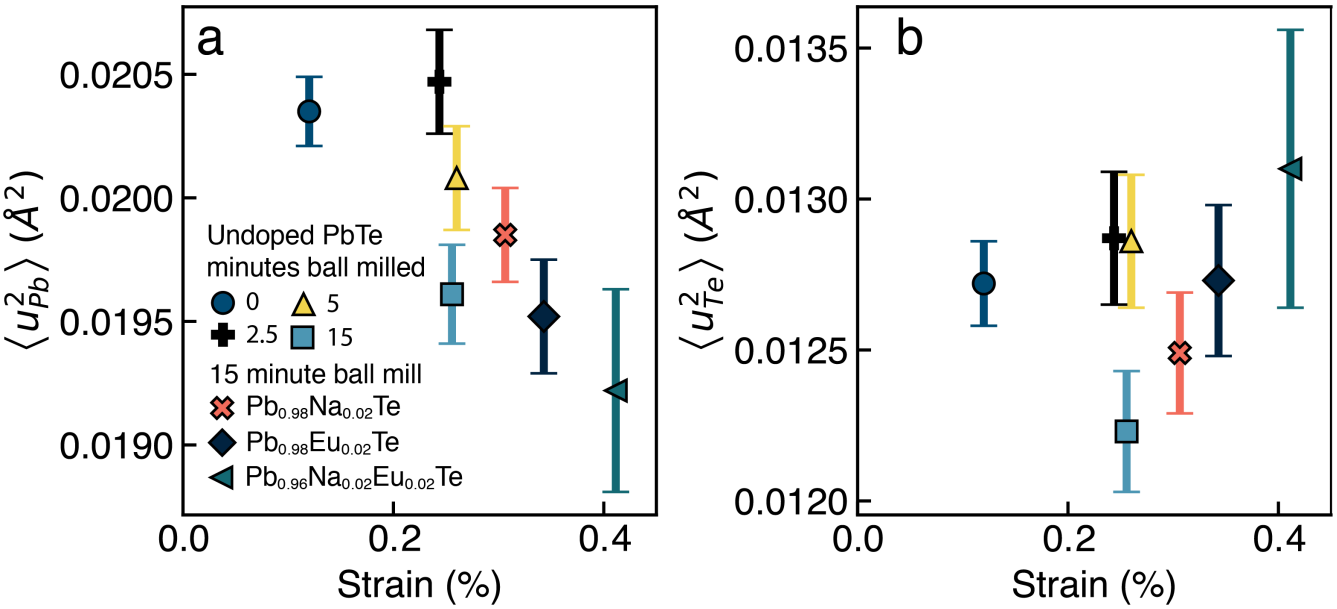

Figure S4. (a) Room temperature isotropic thermal displacement parameters for (a) Pb ($\langle u^2_{Pb}\rangle$) and (b) Te ($\langle u^2_{Te}\rangle$) in undoped PbTe ball milled for 0-15 minutes and Pb doped with Na and/or Eu ball milled for 15 minutes versus strain determined by Rietveld refinement.

S1 Debye temperatures and frequency weighting of different techniques

The Debye phonon dispersion approximation is simple tool for calculating thermodynamic parameters for a material which may, in reality, have a complicated phonon band structure. Experimental θ_D values are calculated from measured cutoff frequencies (ω_D) for a Debye distribution - not the true cutoff frequency of a solid's phonon dispersion. To find θ_D, one measures crystal properties (commonly: speed of sound, heat capacity, or Debye-Waller factors) and relates them to a Debye distribution using

simplified models. In a perfect Debye distribution, each measured property gives identical temperature-independent θ_D. In practice, each technique is weighted differently by phonon frequency i.e., each measurement probes a different n'th moment, $\overline{\omega^n}$, of the phonon density of states ($G(\omega)$), defined as:

$$\overline{\omega^n} \sim \int_0^{\omega_D} \omega^n G(\omega) d\omega \tag{S1}$$

Higher n moments will more heavily weight high frequency phonons and may better capture changes to optical branches in the phonon dispersion. Measurements that probe a lower n will be more sensitive to changes in near-zero frequency phonons and acoustic branches[1]. Therefore, different experiments for finding θ_D are making fundamentally different measurements, and close agreement between the θ_D found by different techniques should not be compared expecting close agreement.

Meticulous explanations distinguishing the moments probed by different measurement techniques are available elsewhere[34–37]. In Table S1, we provide a brief summary of experimental $\theta_{D,PbTe}$, $\theta_{D,Pb}$, and $\theta_{D,Te}$ values measured in other works. We also note where the PbTe-based samples were intentionally prepared to have a high or low degree of internal strain from dislocations ("strained" or "unstrained", respectively), and where the samples were in pellet or powder form. Reduced θ_D values have been measured on strained PbTe samples in pellet form using speed of sound and low temperature heat capacity measurements, which is what one might expect if lattice softening is present and elastic constants are reduced[6–8]. Low temperature heat capacity probes the $n = -3$ moment of the DOS[34]. Speed of sound gives θ_D using an averaging scheme that mirrors $n = -3$, but actually measures the near 0-frequency phonons. Note that, while speed of sound measurements probe low phonon frequencies, anharmonic softening can lead to departures from the heat capacity θ_D at high temperatures and any systematic deviation is dependent on the material and measurement system in question[37]. High temperature Debye-Waller analyses like our study probe the $n = -2$ moment of the DOS, and low temperature Debye-Waller measurements are weighted towards $n = -1$[9,36]. A θ_D approximation using Extended X-ray absorption fine structure analysis (EXAFS) is more complex. In non-Bravais lattice materials, the use of the correlated Debye model is not recommend[10]. Other useful moments of the density of states can be analyzed by the phonon DOS zero point energy ($n = 1$), and high temperature heat capacity ($n = 2$)[36,37]. A measurement's sensitivity to low frequency phonons decreases at higher n. Therefore, measurements like low temperature heat capacity or speed of sound would be best for capturing the effects of long-range strain from dislocations, which may soften low frequency phonons without significant changes at higher frequencies. While more experiments are needed, the lack of softening from neutron powder diffraction atomic displacements suggests that strain primarily softens the lowest frequency phonons in PbTe, or that the character of strain is different between powders and pellets.

Table S1. Collection of Debye temperatures θ_D for Pb, Te, and PbTe found from room temperature speed of sound measurements, low temperature heat capacity, atomic displacement parameters (ADPs) from neutron or X-ray diffraction (XRD) - used in a Debye-Waller analysis - and from an Extended X-ray absorption fine structure (EXAFS) Debye-Waller type analysis. Instances are noted where the PbTe was intentionally strained during synthesis. High temperature specifies measurements taken at $T > \theta_D$ and low temperature is for measurements near 0 K. The moments n of the density of states probed by each method is indicated. Note that θ_D is generally different between each measurement method, but comparable between different measurements using the same method. A softening of elastic constants (reduced θ_D) is apparent from speed of sound and heat capacity measurements, but not an ADP analysis. Uncertainty noted where it is provided in the original works.

Moment (n)	Method	"Strained"?	Temperature	Form	$\theta_{D,Te}$	$\theta_{D,Pb}$	$\theta_{D,PbTe}$
-3	Speed of sound[6]	Yes	High	Pellet	-	-	163
-3	Speed of sound[10]	Yes	High	Pellet	-	-	164
-3	Speed of sound[9]	Yes	High	Pellet	-	-	159
-3	Speed of sound[6]	No	High	Pellet	-	-	172
-3	Speed of sound[13]	No	High	Pellet	-	-	175(3)
-3	Speed of sound[14]	No	High	Pellet	-	-	136
-3	Heat capacity[6]	Yes	Low	Pellet	-	-	135
-3	Heat capacity[6]	No	Low	Pellet	-	-	150
-3	Heat capacity[15]	No	Low	Pellet	-	-	178
-3	Heat capacity[16]	No	Low	Pellet	-	-	168
-2	Neutron powder diffraction ADPs[1]	No	High	Powder	163(1)	102(1)	133(1)
-2	Neutron powder diffraction ADPs[2]	Yes	High	Powder	165(2)	104(1)	134(2)
-2	Neutron single crystal diffraction ADPs[52]	No	High	Pellet	162(3)	101(2)	132(3)
-2	Neutron powder diffraction ADPs[52]	No	High	Powder	157(11)	123(9)	140(14)
-2	Nuclear inelastic scattering ADPs[18]	No	Low	Powder	170(5)	-	-
-2	Synchrotron powder XRD ADPs[40]	No	High	Powder	151(2)	100(1)	125(3)
-2	Neutron powder diffraction ADPs[49]	No	High	Powder	-	104(1)	-
Complex	EXAFS[21]	No	High	Powder	120	116	-
Complex	EXAFS[22]	No	High	Powder	109	121	-

i: This study unstrained, undoped PbTe.
ii: This study, $Pb_{0.98}Na_{0.02}Te$ ball milled 15 minutes

Table S2. Full refinement statistics and crystallographic information determined by Rietveld refinement in the GSAS-II software

Composition	Min Milled	T (K)	a	$U_{iso_{Pb}}$	$U_{iso_{Te}}$	α (x 10^{-5} K^{-1})	wR (%)	GOF	T Cycle
PbTe	0	50	6.433982(15)	0.00337(3)	0.00229(4)	1.82	2.82	3.05	Heating
PbTe	0	100	6.439268(16)	0.00647(5)	0.00389(5)	1.819	1.96	2.5	Heating
PbTe	0	150	6.445108(18)	0.00979(7)	0.00582(7)	1.817	1.95	2.34	Heating
PbTe	0	200	6.451215(20)	0.01315(9)	0.00807(9)	1.815	1.76	2.1	Heating
PbTe	0	250	6.457419(25)	0.01669(12)	0.01024(13)	1.813	2.14	2.21	Heating
PbTe	0	300	6.463733(26)	0.02035(14)	0.01272(14)	1.812	1.8	1.96	Heating
PbTe	0	350	6.469492(32)	0.02383(19)	0.01519(19)	1.81	1.77	1.52	Heating
PbTe	0	400	6.475146(36)	0.02715(24)	0.01717(23)	1.808	2	1.52	Heating
PbTe	0	450	6.480830(40)	0.03035(26)	0.0199(26)	1.807	1.99	1.5	Heating
PbTe	0	500	6.486554(43)	0.03379(31)	0.02211(30)	1.805	1.92	1.48	Heating
PbTe	0	550	6.492170(44)	0.03695(32)	0.02488(32)	1.804	1.92	1.41	Heating
PbTe	0	600	6.497794(49)	0.04004(38)	0.02727(38)	1.802	1.88	1.47	Heating
PbTe	0	519	6.490936(77)	0.03794(61)	0.02381(57)	-	3.12	1.08	Cooling
PbTe	0	472(25)	6.485421(55)	0.03311(39)	0.02179(38)	-	2.48	1.12	Cooling
PbTe	0	422(25)	6.479000(43)	0.0294(28)	0.01922(28)	-	2	1.23	Cooling
PbTe	0	372(25)	6.473183(34)	0.02623(21)	0.01701(21)	-	1.67	1.28	Cooling
PbTe	2.5	300(25)	6.463527(47)	0.02047(21)	0.01287(22)	-	5.66	1.25	Heating
PbTe	5	300	6.463279(50)	0.02008(21)	0.01286(22)	1.821	1.69	1.35	Heating
PbTe	5	350	6.468433(61)	0.02319(28)	0.0148(29)	1.82	1.9	1.2	Heating
PbTe	5	400	6.473956(67)	0.02625(33)	0.01729(34)	1.818	1.89	1.22	Heating
PbTe	5	450	6.479633(68)	0.02968(38)	0.01892(38)	1.816	1.96	1.18	Heating
PbTe	5	500	6.485463(69)	0.03244(42)	0.02167(42)	1.815	1.91	1.21	Heating
PbTe	5	550	6.491301(70)	0.03624(47)	0.02391(47)	1.813	2.05	1.19	Heating
PbTe	5	600	6.497012(72)	0.04002(54)	0.0257(52)	1.812	2.06	1.2	Heating
PbTe	5	650	6.504104(75)	0.04285(57)	0.02956(58)	1.81	2.03	1.23	Heating
PbTe	5	700	6.510339(73)	0.04762(64)	0.03237(63)	1.808	2.15	1.22	Heating
PbTe	5	613	6.506934(149)	0.04554(126)	0.03024(124)	-	3.52	1.06	Cooling
PbTe	5	573(25)	6.496281(122)	0.03908(88)	0.02704(90)	-	3.83	1.06	Cooling
PbTe	5	522(25)	6.490167(88)	0.0357(65)	0.02406(65)	-	3.12	1.09	Cooling
PbTe	5	472(25)	6.484300(68)	0.03261(48)	0.02115(47)	-	2.45	1.1	Cooling
PbTe	5	422(25)	6.478366(48)	0.02883(32)	0.01882(32)	-	1.99	1.14	Cooling
PbTe	5	372(25)	6.472946(40)	0.02573(25)	0.0169(25)	-	1.85	1.2	Cooling
PbTe	15	250(25)	6.456798(42)	0.01672(16)	0.01017(17)	1.854	1.6	1.29	Heating
PbTe	15	300	6.462180(47)	0.01961(20)	0.01223(20)	1.852	1.62	1.27	Heating
PbTe	15	350	6.467860(53)	0.02238(24)	0.01441(24)	1.851	1.61	1.26	Heating
PbTe	15	400	6.473723(58)	0.02589(29)	0.01604(29)	1.849	1.68	1.26	Heating
PbTe	15	450	6.479602(57)	0.02898(31)	0.01885(31)	1.847	1.67	1.23	Heating
PbTe	15	500	6.485345(58)	0.03184(34)	0.02128(34)	1.846	1.57	1.24	Heating
PbTe	15	550	6.491047(58)	0.03552(39)	0.02348(39)	1.844	1.72	1.22	Heating
PbTe	15	600	6.496765(61)	0.03909(43)	0.02587(43)	1.842	1.9	1.27	Heating
PbTe	15	650	6.504921(60)	0.04349(47)	0.02979(47)	1.84	1.83	1.3	Heating
PbTe	15	700	6.510819(61)	0.04729(52)	0.0323(52)	1.838	2.04	1.31	Heating
PbTe	15	622	6.507828(95)	0.04619(80)	0.03146(79)	-	2.48	1.09	Cooling
$Pb_{0.98}Eu_{0.02}Te$	15	300(25)	6.466538(61)	0.01952(23)	0.01273(25)	1.757	5.13	1.36	Heating
$Pb_{0.98}Eu_{0.02}Te$	15	350	6.472092(90)	0.0231(41)	0.0142(41)	1.755	1.34	1.17	Heating
$Pb_{0.98}Eu_{0.02}Te$	15	400	6.477824(95)	0.02528(42)	0.01708(45)	1.754	1.58	1.15	Heating
$Pb_{0.98}Eu_{0.02}Te$	15	450	6.483549(98)	0.02796(47)	0.01932(51)	1.752	1.29	1.16	Heating
$Pb_{0.98}Eu_{0.02}Te$	15	500	6.489187(97)	0.03163(55)	0.02201(59)	1.751	1.32	1.16	Heating
$Pb_{0.98}Eu_{0.02}Te$	15	550	6.494918(99)	0.03521(62)	0.02372(63)	1.749	1.27	1.15	Heating
$Pb_{0.98}Eu_{0.02}Te$	15	600	6.500565(103)	0.03922(75)	0.0255(74)	1.748	1.65	1.12	Heating
$Pb_{0.98}Na_{0.02}Te$	15	50	6.431687(28)	0.00345(4)	0.00265(6)	1.895	1.51	1.58	Heating
$Pb_{0.98}Na_{0.02}Te$	15	100	6.436746(31)	0.00633(6)	0.00404(8)	1.894	1.46	1.54	Heating
$Pb_{0.98}Na_{0.02}Te$	15	150	6.442475(36)	0.00952(9)	0.00581(10)	1.892	1.34	1.49	Heating
$Pb_{0.98}Na_{0.02}Te$	15	200	6.448444(38)	0.01288(12)	0.00791(13)	1.89	1.67	1.35	Heating
$Pb_{0.98}Na_{0.02}Te$	15	250	6.454530(42)	0.01642(15)	0.01019(16)	1.889	1.27	1.3	Heating

Table S2 continued from previous page

Composition	Min Milled	T (K)	a	$U_{iso_{Pb}}$	$U_{iso_{Te}}$	α (x 10^{-5} K^{-1})	wR (%)	GOF	T Cycle
$Pb_{0.98}Na_{0.02}Te$	15	300	6.460557(48)	0.01985(19)	0.01249(20)	1.887	1.39	1.3	Heating
$Pb_{0.98}Na_{0.02}Te$	15	350	6.466384(60)	0.02324(27)	0.01461(28)	1.885	1.48	1.19	Heating
$Pb_{0.98}Na_{0.02}Te$	15	400	6.472293(64)	0.02574(31)	0.0166(31)	1.883	1.48	1.17	Heating
$Pb_{0.98}Na_{0.02}Te$	15	450	6.478449(64)	0.02901(34)	0.01942(35)	1.882	1.61	1.24	Heating
$Pb_{0.98}Na_{0.02}Te$	15	500	6.484719(57)	0.03299(38)	0.02152(38)	1.88	1.62	1.22	Heating
$Pb_{0.98}Na_{0.02}Te$	15	550	6.490691(58)	0.03607(42)	0.02376(42)	1.878	1.74	1.25	Heating
$Pb_{0.98}Na_{0.02}Te$	15	600	6.496541(58)	0.03898(44)	0.02625(44)	1.876	1.76	1.23	Heating
$Pb_{0.98}Na_{0.02}Te$	15	650	6.504927(60)	0.04483(51)	0.02991(50)	1.874	1.7	1.23	Heating
$Pb_{0.98}Na_{0.02}Te$	15	700	6.510879(64)	0.04821(56)	0.03303(56)	1.872	1.93	1.26	Heating
$Pb_{0.98}Na_{0.02}Te$	15	656	6.509827(191)	0.04867(178)	0.03047(173)	-	7.31	1.04	Cooling
$Pb_{0.98}Na_{0.02}Te$	15	622(25)	6.507282(90)	0.0467(78)	0.03165(78)	-	2.65	1.06	Cooling
$Pb_{0.98}Na_{0.02}Te$	15	572(25)	6.501878(74)	0.04369(62)	0.02925(61)	-	2.15	1.11	Cooling
$Pb_{0.98}Na_{0.02}Te$	15	522(25)	6.495688(60)	0.04031(50)	0.02598(48)	-	1.95	1.14	Cooling
$Pb_{0.98}Na_{0.02}Te$	15	472(25)	6.488785(45)	0.03517(32)	0.0237(32)	-	1.87	1.18	Cooling
$Pb_{0.98}Na_{0.02}Te$	15	432(25)	6.481133(63)	0.0303(38)	0.02046(38)	-	1.54	1.24	Cooling
$Pb_{0.98}Na_{0.02}Te$	15	378(25)	6.471440(49)	0.02513(32)	0.01601(32)	-	1.81	1.14	Cooling
$Pb_{0.96}Na_{0.02}Eu_{0.02}Te$	15	300(25)	6.463869(113)	0.01922(41)	0.0131(46)	1.875	1.35	1.14	Heating
$Pb_{0.96}Na_{0.02}Eu_{0.02}Te$	15	350	6.469409(104)	0.02267(44)	0.01429(46)	1.873	6.43	1.15	Heating
$Pb_{0.96}Na_{0.02}Eu_{0.02}Te$	15	400	6.475279(103)	0.02562(48)	0.01599(50)	1.872	1.49	1.13	Heating
$Pb_{0.96}Na_{0.02}Eu_{0.02}Te$	15	450	6.481236(96)	0.02878(52)	0.01884(54)	1.87	1.48	1.14	Heating
$Pb_{0.96}Na_{0.02}Eu_{0.02}Te$	15	500	6.487262(94)	0.03244(59)	0.02132(59)	1.868	1.61	1.19	Heating
$Pb_{0.96}Na_{0.02}Eu_{0.02}Te$	15	550	6.493239(91)	0.03633(69)	0.02253(67)	1.867	1.94	1.14	Heating
$Pb_{0.96}Na_{0.02}Eu_{0.02}Te$	15	600	6.498830(91)	0.03827(65)	0.02671(68)	1.865	1.32	1.14	Heating
$Pb_{0.96}Na_{0.02}Eu_{0.02}Te$	15	650	6.507002(96)	0.04484(82)	0.02939(84)	1.863	2.04	1.16	Heating
$Pb_{0.96}Na_{0.02}Eu_{0.02}Te$	15	700	6.511804(98)	0.04962(99)	0.031(94)	1.861	1.95	1.2	Heating
$Pb_{0.96}Na_{0.02}Eu_{0.02}Te$	15	666	6.510520(257)	0.04721(232)	0.03035(230)	-	4.05	1.07	Cooling
$Pb_{0.96}Na_{0.02}Eu_{0.02}Te$	15	622(25)	6.507626(179)	0.04618(162)	0.02956(158)	-	2.81	1.04	Cooling
$Pb_{0.96}Na_{0.02}Eu_{0.02}Te$	15	576(25)	6.495425(269)	0.03683(171)	0.027(188)	-	4.01	1.05	Cooling
$Pb_{0.96}Na_{0.02}Eu_{0.02}Te$	15	522(25)	6.489328(182)	0.03502(136)	0.02254(136)	-	3.37	1.05	Cooling
$Pb_{0.96}Na_{0.02}Eu_{0.02}Te$	15	472(25)	6.483498(139)	0.03084(91)	0.02113(95)	-	2.6	1.06	Cooling
$Pb_{0.96}Na_{0.02}Eu_{0.02}Te$	15	422(25)	6.477474(100)	0.02794(61)	0.0194(65)	-	2.44	1.08	Cooling
$Pb_{0.96}Na_{0.02}Eu_{0.02}Te$	15	372(25)	6.471786(78)	0.02515(49)	0.01638(49)	-	1.65	1.09	Cooling

Table S3. Full refinement statistics and strain information determined by Rietveld refinement in the GSAS-II software

Composition	Min Milled	T (K)	S400	S220	μstrain	T Cycle
PbTe	0	50	378.4(18.1)	564.8(18.6)	955.5	Heating
PbTe	0	100	497.6(21.2)	696.7(20.8)	1079.5	Heating
PbTe	0	150	544.2(25.1)	734.5(23.8)	1120.6	Heating
PbTe	0	200	533.4(26.3)	787.1(25.2)	1137.1	Heating
PbTe	0	250	660.4(34.8)	772.1(32.3)	1197.2	Heating
PbTe	0	300	596.1(34.0)	859.2(32.0)	1199.4	Heating
PbTe	0	350	556.2(41.2)	935.3(38.3)	1209.4	Heating
PbTe	0	400	615.5(47.6)	872.4(42.6)	1217.9	Heating
PbTe	0	450	647.1(52.7)	785.7(44.1)	1204.3	Heating
PbTe	0	500	532.0(51.3)	812.2(45.5)	1158.4	Heating
PbTe	0	550	541.0(53.8)	746.4(45.0)	1140	Heating
PbTe	0	600	460.9(56.5)	785.9(49.7)	1114.9	Heating
PbTe	0	519(25)	599.7(95.4)	585.1(72.1)	1107.7	Cooling
PbTe	0	472(25)	491.5(63.2)	729.5(53.3)	1104.8	Cooling
PbTe	0	422(25)	553.6(53.4)	823.0(48.4)	1170.8	Cooling
PbTe	0	372(25)	524.5(41.3)	746.4(36.1)	1124.7	Cooling
PbTe	2.5	300	1929.5(112.3)	4272.3(116.5)	2437.5	Heating
PbTe	5	300	2241.4(128.3)	4809.5(131.3)	2601.7	Heating
PbTe	5	350	2278.6(159.1)	4736.6(155.6)	2602.1	Heating
PbTe	5	400	2125.8(168.9)	4699.4(166.3)	2565.5	Heating

Table S3 continued from previous page

Composition	Min Milled	T (K)	S400	S220	μstrain	T Cycle
PbTe	5	450	1899.8(160.6)	4018.5(153.5)	2396.9	Heating
PbTe	5	500	1498.7(146.6)	3014.7(137.1)	2100.6	Heating
PbTe	5	550	1170.1(130.0)	2396.6(120.8)	1887.8	Heating
PbTe	5	600	943.1(119.7)	1870.7(108.6)	1665.3	Heating
PbTe	5	650	680.0(105.8)	1384.4(98.1)	1428.2	Heating
PbTe	5	700	476.8(86.9)	816.7(73.0)	1139.8	Heating
PbTe	5	613(25)	575.8(110.8)	685.1(89.4)	1131.9	Cooling
PbTe	5	573(25)	567.7(83.7)	696.3(67.7)	1133.1	Cooling
PbTe	5	522(25)	590.5(154.3)	910.1(125.5)	1113.7	Cooling
PbTe	5	472(25)	468.3(170.1)	764.7(143.0)	1227.2	Cooling
PbTe	5	422(25)	512.5(57.5)	724.2(49.0)	1111.6	Cooling
PbTe	5	372(25)	523.7(48.4)	636.0(41.5)	1080.8	Cooling
PbTe	15	250	2399.8(123.8)	4331.1(120.4)	2513.3	Heating
PbTe	15	300	2581.3(143.3)	4639.8(135.9)	2556.8	Heating
PbTe	15	350	2686.4(162.5)	4495.1(142.8)	2653.4	Heating
PbTe	15	400	2165.1(142.8)	3526.9(122.1)	2657.8	Heating
PbTe	15	450	1725.6(128.6)	2717.2(111.5)	2372.9	Heating
PbTe	15	500	1381.3(115.9)	2151.3(99.6)	2102.7	Heating
PbTe	15	550	1086.5(104.2)	1477.3(82.3)	1879.1	Heating
PbTe	15	600	2256.4(109.9)	4293.8(108.4)	1611.9	Heating
PbTe	15	650	769.5(88.1)	939.0(69.6)	1324.6	Heating
PbTe	15	700	712.2(255.5)	763.1(182.3)	1134.7	Heating
PbTe	15	622(25)	440.5(106.7)	680.7(85.5)	1064.4	Cooling
$Pb_{0.98}Eu_{0.02}Te$	15	300	4484.0(221.6)	7537.3(202.3)	3430.5	Heating
$Pb_{0.98}Eu_{0.02}Te$	15	350	4708.4(339.1)	7668.2(297.4)	3490.9	Heating
$Pb_{0.98}Eu_{0.02}Te$	15	400	4419.8(345.2)	7486.5(305.1)	3425	Heating
$Pb_{0.98}Eu_{0.02}Te$	15	450	4013.5(340.0)	6135.6(287.3)	3179.9	Heating
$Pb_{0.98}Eu_{0.02}Te$	15	500	2891.5(288.3)	4879.7(248.6)	2777.2	Heating
$Pb_{0.98}Eu_{0.02}Te$	15	550	2771.8(283.8)	3982.7(231.3)	2609.4	Heating
$Pb_{0.98}Eu_{0.02}Te$	15	600	2286.9(271.6)	3252.3(213.7)	2368	Heating
$Pb_{0.98}Na_{0.02}Te$	15	50	2132.2(73.3)	5722.0(90.5)	2698.8	Heating
$Pb_{0.98}Na_{0.02}Te$	15	100	3006.3(92.2)	6461.6(103.8)	2989.9	Heating
$Pb_{0.98}Na_{0.02}Te$	15	150	3354.7(112.7)	6740.8(120.5)	3100.3	Heating
$Pb_{0.98}Na_{0.02}Te$	15	200	3459.7(122.7)	6842.4(123.9)	3139.4	Heating
$Pb_{0.98}Na_{0.02}Te$	15	250	3115.9(129.5)	6624.7(130.2)	3050.6	Heating
$Pb_{0.98}Na_{0.02}Te$	15	300	3231.4(147.9)	6515.8(146.8)	3063.1	Heating
$Pb_{0.98}Na_{0.02}Te$	15	350	3542.9(197.9)	6725.0(185.3)	3156.3	Heating
$Pb_{0.98}Na_{0.02}Te$	15	400	3368.0(204.7)	6207.8(186.7)	3056.9	Heating
$Pb_{0.98}Na_{0.02}Te$	15	450	2442.4(169.1)	3678.5(146.1)	2467	Heating
$Pb_{0.98}Na_{0.02}Te$	15	500	1346.6(112.1)	1903.4(94.1)	1805.4	Heating
$Pb_{0.98}Na_{0.02}Te$	15	550	1017.1(98.4)	1459.8(82.6)	1578.2	Heating
$Pb_{0.98}Na_{0.02}Te$	15	600	744.3(84.2)	1179.9(71.2)	1388.3	Heating
$Pb_{0.98}Na_{0.02}Te$	15	650	568.4(77.5)	938.8(65.2)	1229.9	Heating
$Pb_{0.98}Na_{0.02}Te$	15	700	540.7(80.2)	756.9(62.8)	1150.4	Heating
$Pb_{0.98}Na_{0.02}Te$	15	656(25)	446.7(217.8)	836.5(189.6)	1131.4	Cooling
$Pb_{0.98}Na_{0.02}Te$	15	622(25)	496.3(71.3)	901.7(62.1)	1131.6	Cooling
$Pb_{0.98}Na_{0.02}Te$	15	572(25)	612.4(63.7)	530.8(50.5)	1159.5	Cooling
$Pb_{0.98}Na_{0.02}Te$	15	522(25)	1318.3(116.6)	1331.6(86.9)	1177	Cooling
$Pb_{0.98}Na_{0.02}Te$	15	472(25)	681.0(60.3)	771.1(48.0)	1218.6	Cooling
$Pb_{0.98}Na_{0.02}Te$	15	432(25)	513.1(88.5)	826.3(73.0)	1649	Cooling
$Pb_{0.98}Na_{0.02}Te$	15	378(25)	490.2(105.5)	780.2(88.4)	1086.4	Cooling
$Pb_{0.96}Na_{0.02}Eu_{0.02}Te$	15	300	5549.5(472.3)	12068.4(462.2)	4114.4	Heating
$Pb_{0.96}Na_{0.02}Eu_{0.02}Te$	15	350	6445.5(467.2)	12047.9(423.9)	4242.2	Heating
$Pb_{0.96}Na_{0.02}Eu_{0.02}Te$	15	400	5484.7(424.3)	10806.6(388.0)	3981.3	Heating
$Pb_{0.96}Na_{0.02}Eu_{0.02}Te$	15	450	3830.1(327.8)	6407.2(286.5)	3180.8	Heating
$Pb_{0.96}Na_{0.02}Eu_{0.02}Te$	15	500	2712.5(268.9)	4125.7(228.5)	2613.7	Heating
$Pb_{0.96}Na_{0.02}Eu_{0.02}Te$	15	550	2043.6(229.7)	3408.7(196.6)	2330.1	Heating

Table S3 continued from previous page

Composition	Min Milled	T (K)	S400	S220	μstrain	T Cycle
$Pb_{0.96}Na_{0.02}Eu_{0.02}Te$	15	600	1608.6(203.6)	2662.7(170.6)	2066.5	Heating
$Pb_{0.96}Na_{0.02}Eu_{0.02}Te$	15	650	1278.0(189.7)	1751.8(148.7)	1757.2	Heating
$Pb_{0.96}Na_{0.02}Eu_{0.02}Te$	15	700	968.1(170.8)	1263.5(131.9)	1513.1	Heating
$Pb_{0.96}Na_{0.02}Eu_{0.02}Te$	15	666(25)	887.4(428.8)	1767.9(389.2)	1624.3	Cooling
$Pb_{0.96}Na_{0.02}Eu_{0.02}Te$	15	622(25)	767.0(274.0)	1427.9(245.2)	1479	Cooling
$Pb_{0.96}Na_{0.02}Eu_{0.02}Te$	15	576(25)	1663.8(579.5)	1666.8(412.9)	1857.9	Cooling
$Pb_{0.96}Na_{0.02}Eu_{0.02}Te$	15	522(25)	959.8(302.4)	1406.0(256.7)	1540.5	Cooling
$Pb_{0.96}Na_{0.02}Eu_{0.02}Te$	15	472(25)	1030.8(240.3)	1414.8(203.4)	1567.3	Cooling
$Pb_{0.96}Na_{0.02}Eu_{0.02}Te$	15	422(25)	995.5(167.6)	1226.9(138.3)	1497.4	Cooling
$Pb_{0.96}Na_{0.02}Eu_{0.02}Te$	15	372(25)	985.6(132.4)	1193.2(111.9)	1481.1	Cooling

References

1. Matsunaga, T. *et al.* Phase-change materials: Vibrational softening upon crystallization and its impact on thermal properties. *Adv. Funct. Mater.* **21**, 2232–2239, DOI: 10.1002/adfm.201002274 (2011).
2. Barron, T. H. K. & Morrison, J. A. On the specific heat of solids at low temperatures. *Can. J. Phys.* **35**, 799–810, DOI: 10.1139/p57-088 (1957).
3. Barron, T. H. K., Leadbetter, A. J., Morrison, J. A. & Salter, L. S. The calculation of Debye-Waller factors from thermodynamic data. In *Inelastic Scattering of Neutrons in Solids and Liquids*, 49–57 (1962).
4. Barron, T. H. K., Leadbetter, A. J., Morrison, J. A. & Salter, L. S. Temperature factors and thermodynamic properties of crystals. *Acta Crystallogr.* **20**, 125–131, DOI: 10.1107/s0365110x66000227 (1966).
5. Grimvall, G. Thermophysical Properties of Materials - Enlarged and revised edition. 89–97 (Elsevier Science B.V., 1999).
6. Hanus, R. *et al.* Lattice Softening Significantly Reduces Thermal Conductivity and Leads to High Thermoelectric Efficiency. *Adv. Mater.* **31**, 1900108, DOI: 10.1002/adma.201900108 (2019).
7. Slade, T. J. *et al.* Contrasting SnTe-NaSbTe2and SnTe-NaBiTe2Thermoelectric Alloys: High Performance Facilitated by Increased Cation Vacancies and Lattice Softening. *J. Am. Chem. Soc.* **142**, 12524–12535, DOI: 10.1021/jacs.0c05650 (2020).
8. Tan, G. *et al.* High Thermoelectric Performance in SnTe- AgSbTe 2 Alloys from Lattice Softening, Giant Phonon-Vacancy Scattering, and Valence Band Convergence. *ACS Energy Lett.* **3**, 705–712, DOI: 10.1021/acsenergylett.8b00137 (2018).
9. Blackman, M. A Note on the Debye-Waller Theory. *Acta Crystallogr. Sect. A* **9**, 734 (1956).
10. Vaccari, M. & Fornasini, P. Einstein and Debye models for EXAFS parallel and perpendicular mean-square relative displacements. *J. Synchrotron Radiat.* **13**, 321–325, DOI: 10.1107/S0909049506018504 (2006).
11. Wu, Y. *et al.* Lattice Strain Advances Thermoelectrics. *Joule* **3**, 1276–1288, DOI: 10.1016/j.joule.2019.02.008 (2019).
12. Wu, Y. *et al.* Manipulation of Band Degeneracy and Lattice Strain for Extraordinary PbTe Thermoelectrics. *Research* **2020**, 1–12, DOI: 10.34133/2020/8151059 (2020).
13. Houston, B., Strakna, R. E. & Belson, H. S. Elastic constants, thermal expansion, and Debye temperature of lead telluride. *J. Appl. Phys.* **39**, 3913–3916, DOI: 10.1063/1.1656874 (1968).
14. Pei, Y. L. & Liu, Y. Electrical and thermal transport properties of Pb-based chalcogenides: PbTe, PbSe, and PbS. *J. Alloy. Compd.* **514**, 40–44, DOI: 10.1016/j.jallcom.2011.10.036 (2012).
15. Nouneh, K. *et al.* Influence of an electron-phonon subsystem on specific heat and two-photon absorption of the semimagnetic semiconductors Pb1-x Ybx X (X=S, Se,Te) near the semiconductor-isolator phase transformation. *Phys. Rev. B - Condens. Matter Mater. Phys.* **73**, 4–11, DOI: 10.1103/PhysRevB.73.035329 (2006).
16. Matsushita, Y., Wianecki, P. A., Sommer, A. T., Geballe, T. H. & Fisher, I. R. Type II superconducting parameters of Tl-doped PbTe determined from heat capacity and electronic transport measurements. *Phys. Rev. B - Condens. Matter Mater. Phys.* **74**, 1–6, DOI: 10.1103/PhysRevB.74.134512 (2006).
17. Li, C. W. *et al.* Anharmonicity and atomic distribution of SnTe and PbTe thermoelectrics. *Phys. Rev. B - Condens. Matter Mater. Phys.* **90**, 214303, DOI: 10.1103/PhysRevB.90.214303 (2014).
18. Bauer Pereira, P. *et al.* Lattice dynamics and structure of GeTe, SnTe and PbTe. *Phys. Status Solidi (B) Basic Res.* **250**, 1300–1307, DOI: 10.1002/pssb.201248412 (2013).
19. Christensen, S., Bindzus, N., Sist, M., Takata, M. & Iversen, B. B. Structural disorder, anisotropic micro-strain and cation vacancies in thermo-electric lead chalcogenides. *Phys. Chem. Chem. Phys.* **18**, 15874–15883, DOI: 10.1039/c6cp01730d (2016).

20. Božin, E. S. *et al.* Entropically stabilized local dipole formation in lead chalcogenides. *Science* **330**, 1660–1663, DOI: 10.1126/science.1192759 (2010).

21. Keiber, T., Bridges, F. & Sales, B. C. Lead is not off center in PbTe: The importance of r-space phase information in extended x-ray absorption fine structure spectroscopy. *Phys. Rev. Lett.* **111**, 1–5, DOI: 10.1103/PhysRevLett.111.095504 (2013).

22. Bridges, F., Keiber, T., Medling, S. & Sales, B. C. Unusual distortion about Tl and Pb in PbTe:Tl. *Phys. Stat. Sol. (C)* **10**, 236–241, DOI: 10.1002/pssc.201200478 (2013).

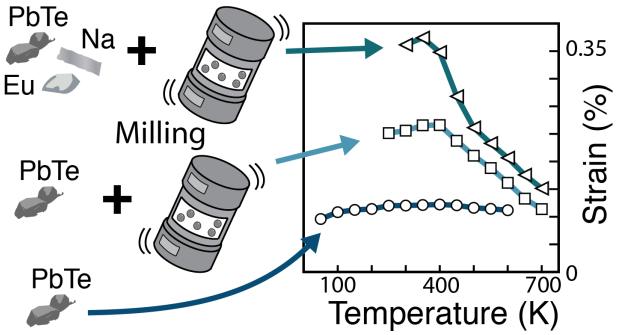

Figure S5. TOC Figure